Nanoscale

Direct Synthesis of Pure Single-Crystalline Magnéli Phase Ti8O15 Nanowires as Conductive Carbon-Free Material for Electrocatalysis

Journal:	*Nanoscale*
Manuscript ID:	NR-COM-10-2014-005806.R1
Article Type:	Communication
Date Submitted by the Author:	19-Dec-2014
Complete List of Authors:	He, Chunyong; Sun Yat-sen University, Chang, Shiyong; Sun Yat-sen University, Huang, Xiangdong; Guangzhou Automobile Group Co., Ltd, Wang, Qingquan; Guangzhou Automobile Group Co., Ltd, Mei, Ao; Guangzhou Automobile Group Co., Ltd, Shen, Pei; Sun Yat-sen University,

Nanoscale

RSCPublishing

COMMUNICATION

Direct Synthesis of Pure Single-Crystalline Magnéli Phase Ti_8O_{15} Nanowires as Conductive Carbon-Free Material for Electrocatalysis

Cite this: DOI: 10.1039/x0xx00000x

Received 00th January 2012,
Accepted 00th January 2012

DOI: 10.1039/x0xx00000x

www.rsc.org/

Chunyong He,[1†] Shiyong Chang,[1,2†] Xiangdong Huang,[2,*] Qingquan Wang,[2] Ao Mei[2] and Pei Kang Shen[1,*]

Keywords: Magnéli Phase, Ti_8O_{15} Nanowires, Conductive, Carbon-Free, Electrocatalysis.

The Magnéli phase Ti_8O_{15} nanowires (NWs) have been grown directly on Ti substrate by a facile one-step evaporation-deposition synthesis method in hydrogen atmosphere. The Ti_8O_{15} NWs exhibit outstanding electrical conductivity at room temperature. The electrical conductivity of a single Ti_8O_{15} nanowire is 20.6 S/cm at 300 K. Theoretical calculations manifest that the existence of a large number of oxygen vacancies changes the band structure, resulting in the reduction of the electronic resistance. The Magnéli phase Ti_8O_{15} nanowires have been used as conductive carbon-free support to load Pt nanoparticles for direct methanol oxidation reaction (MOR). The Pt/Ti_8O_{15} NWs show an enhanced activity and extremely high durability compared with commercial Pt/C catalyst.

Introduction

Magnéli phases of titanium oxides, also called reduced titanium oxides or black titanium oxides, comprise a series of different compounds having the generic formula Ti_nO_{2n-1} ($3 \le n \le 10$).[1-3] These materials have been generally used as visible light-absorptive catalysts, catalyst support and battery electrode materials owning to their high electrical conductivity and unique composition and structures.[4-9]

Traditionally, the Magnéli phase Ti_8O_{15} is synthesized by the thermal reduction of TiO_2 powders at high temperature with H_2 gas or other reductants.[1,10-12] This two steps synthesis strategy inevitably leads to the agglomeration of nanoparticles.[13] Han *et al*. prepared Magnéli phase titanium oxides nanowires by heating $H_2Ti_3O_7$ nanorods at 800–1050 °C under a hydrogen atmosphere.[14] However, the nanostructure of the precursor was partially destroyed by the high-temperature treatment. Recently, Tominaka *et al*. successfully synthesized Ti_2O_3 nanoparticles by reducing TiO_2 nanopaticles in CaH_2, a strong reducing agent, at 350 °C for 15 days.[8] The Ti_2O_3 nanoparticles maintained the same particle size as the parent TiO_2. The bad news is this method requires harsh experimental conditions and long reaction times, and is not suitable for other nanostructure synthesis.

The limited durability of the carbon-supported catalysts has been realized mainly due to the electrochemical corrosion of the carbon supporting material. [15] Many progressive works have been achieved on the exploration of carbon-free supporting materials in the past decades, including nitride,[16] carbide,[16,17] mesoporous silicas,[18] and as well as metal oxides.[19-22] Due to the superior chemical stability under reducing and oxidizing conditions, TiO_2 has been considered as potential support of the precious metal nanoparticles.[19,23] However, the use of these metal oxides as electrocatalyst supporting materials is limited since their intrinsic low electrical conductivity.[24] In this paper, we demonstrate a facile one-step evaporation-deposition synthesis method to produce conductive well-defined Ti_nO_{2n-1} (n=8) nanowires (NWs). The as-prepared Ti_8O_{15} NWs exhibited a very high electrical conductivity at room temperature (20.6 S/cm). The conductive Ti_8O_{15} NWs is a potential supporting material to load metal nanoparticles for alcohol oxidation. The Pt-/Ti_8O_{15} NWs showed significantly enhanced electrocatalytic performance and extremely high durability for methanol oxidation.

Experimental section

Synthesis of Ti_8O_{15} nanowires.

Synthesis of Ti_8O_{15} nanowires was carried out in a conventional tube furnace (figure S1A). Commercial Ti (Grade 1, purity 99.5%) foil sized 2.5cm× 3.0cm× 0.5mm (width× length × thickness) were used as substrate.The Ti foil chemically polished with HF:HNO_3:H_2O(1:3:6) solution for 5s to remove the native surface oxide layer and then ultrasonically cleaned in acetone, ethanol and deionized water for 10 min, respectively. A quartz boat loaded pure TiO_2 powders (99.0%, 5-10nm, 2 g) was placed at the center of the tube and the Ti substrate located 6 cm from the boat .The reaction system was flushed with N_2 several times to remove residual oxygen and moisture and then heated at a rate of 8°C min^{-1} to 1050 °C and kept for 2 h with hydrogen gas flow rate 20ml min^{-1}. Then, the furnace was cooled at a rate of 5°C min^{-1} to room temperature. Finally, a layer of black material was observed on the surface of the Ti substrate (figure S1B).

Preparation of Pt/Ti_8O_{15} NWs electrocatalysts.

The Pt/Ti_8O_{15} NWs electrocatalyst was prepared by pulsed electrodeposition with a three-electrode electrochemical cell. The Pt nanoparticles were electrodeposited on the Ti_8O_{15} NWs (acted as working electrode) via a pulse-mode potentiostatic approach in a thermostat-controlled standard three-electrode cell at 30 ^oC, with a saturated calomel electrode (SCE) as the reference electrode, a piece of platinum plate electrode (1×1 cm^{-2}) as the counter electrode. For the electrodeposition of Pt, 0.2 mM H_2PtCl_6 were formulated in aqueous citric acid (CA) solutions (0.15 M) as precursors. The pH values of all deposition electrolytes were controlled between 1.9 and 2.2. The deposition electrolyte was saturated with argon gas during the deposition processes under magnetic stirring. The Pt nanoparticles were electrodeposited at a fixed holding time of 0.2 s at high potential (0V vs. SCE) and 2.5 s at low potential (-1.2V vs. SCE) for 120 cycles. After that, the Pt/Ti_8O_{15} NWs was thoroughly rinsed with deionized water. Pt/TiO_2 was also prepared by the some method for comparison

Materials Characterizations.

X-ray diffraction (XRD) analysis was performed on a D8 ADVANCE powder X-ray diffractometer (Cu Kα, 30 kV, 30 mA). X-ray photoelectron spectroscopy (XPS) was done with a Thermo VG Scientific Sigma Probe spectrometer. Scanning electron microscope (SEM) were carried out on thermal field emission environmental SEM-ED-EBSD (Quanta 400F, FEI, Oxford, HKL Ltd.). The high-resolution transmission electron microscope (HRTEM) and High-angle annular dark-field scanning transmission electron microscopy-energy dispersive spectroscopy HAADF-STEM-EDS elements mapping were performed using a Tecnai G2 F30 (FEI) operating at 300 kV. The X-ray photoelectron spectroscopy (XPS) measurements were carried out on a XPS apparatus (ESCALAB 250, Thermo-VG Scientific Ltd.). The loadings of Pt were measured by an inductively coupled plasma-atomic emission spectrometry, ICP-AES (IRIS(HR), USA).

Electrochemical measurements.

An Bio-logic VMP3 electrochemical work station (France) was employed to perform the electrochemical measurements in a thermostat-controlled standard three-electrode cell at 30 ^oC with a saturated calomel electrode (SCE) as the reference electrode, a platinum foil (1.0×1.0 cm^{-2}) as the counter electrode. The methanol oxidation reaction (MOR) of the Pt/Ti_8O_{15} NWs electrocatalyst was carried out in an nitrogen - saturated 0.5 mol L^{-1} H_2SO_4+1.0 mol $L^{-1}CH_3OH$ solution. The cyclic voltammograms (CVs) were test at the scan rate of 0.02 V s^{-1} within the potential window of -0.2 to 0.95 V *vs.* SCE. The durability of the Pt/Ti_8O_{15} NWs for MOR was measured by performing CVs of Pt/Ti_8O_{15} NWs over 6,000 cycles using the the scan rate of 0.1 V s^{-1} from -0.2 V to 0.95 V.

The 46.7 wt% platinum on carbon catalyst (Pt/C from TKK, Japan) was measured for comparison. The catalyst ink was prepared as follows. Pt/C (5.0 mg) and 0.5 mL Nafion solution (0.05 wt %, DuPont, USA) solution were dispersed in 0.5 ml of ethanol by sonication for an hour to form a well-dispersed ink. A certain amount of the ink was transferred onto the surface of the glassy carbon electrode. After dried under infrared lamp for 5 min, a catalyst thin film was obtained. Other experimental conditions were the same as for the Pt/Ti_8O_{15} NWs catalyst.

The measured loadings of the Pt on the prepared Pt/Ti_8O_{15} NWs electrode was 0.067 mg cm^{-2}. And we kept the same loadings on Pt/C electrode.

Results and discussion

Figure 1 shows the X-ray diffraction (XRD) patterns of the Ti_8O_{15} product (red), Ti substrate (blue) and anatase TiO_2 powders (black) used in the experiments. From **Figure 1**A, it is obvious that the Ti_8O_{15} product has distinguished diffraction peaks of Ti_8O_{15} except for the characteristic peak at 2θ=70.66° from Ti substrate. None of anatase TiO_2 diffraction peaks can be observed in this product. **Figure 1**B enlarges the XRD pattern in the 2θ range from 25° to 45°. The characteristic peaks in spectrum further confirmed that the product is triclinic Ti_8O_{15} (JCPDF, No. 50-0790). **Figure 1**C illustrates the crystal structure of anatase structured TiO_2. It is well known that the anatase TiO_2 has an edge-shared distorted TiO_6 octahedra structure. Compared with the structure of anatase TiO_2, triclinic structured Ti_8O_{15} has the same structure but every eighth layer having oxygen atoms missing to accommodate for the loss in stoichiometry (see **Figure 1**D).

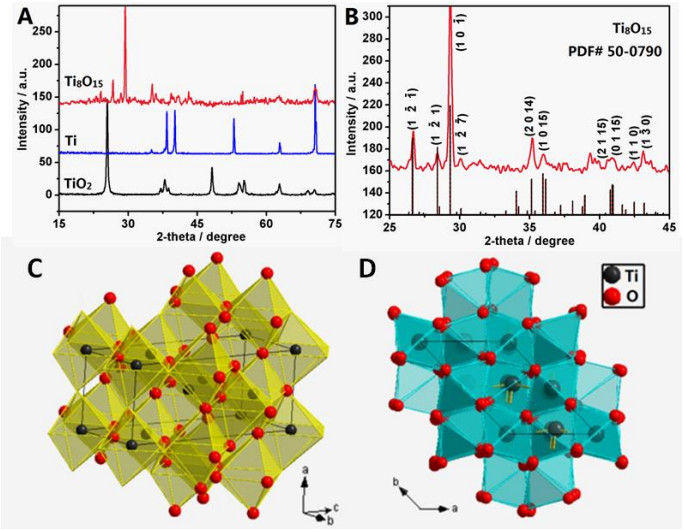

Figure 1. (A) XRD patterns of the Ti_8O_{15} product, Ti substrate and anatase TiO_2 powder. (B) Enlarged XRD pattern of Ti_8O_{15}. Schematic illustration of crystal structures of titanium oxides. (C) Anatase structured TiO_2 and (D) triclinic structured Ti_8O_{15} viewed along the c-axis and in perspective.

The morphologies of the Ti_8O_{15} NWs are characterized by the scanning electron microscope (SEM) and transmission electron microscope (TEM). **Figure 2**A-C show the SEM images of the Ti_8O_{15} NWs at different magnifications, indicating the highly uniform and densely packed array of these nanowires. The inset in **Figure 2**A is a digital photo of the sample, it can be clearly seen that the surface of the Ti sheet was completely covered by a black layer. The cross-view SEM image (**Figure 2**C) indicates that these nanowires have lengths of up to micrometer level. **Figure 2**D-F show TEM images of the Ti_8O_{15} NWs at different magnifications. **Figure 2**E shows that the products are relatively straight nanowires with diameter about 30 nm. The inset in **Figure 2**E is the corresponding selected area electron diffraction (SAED) pattern, which was collected from the head of a nanowire as indicated by the red cycle. High-resolution transmission electron microscopy (HRTEM) image is shown in **Figure 2**F. Two lattice plane distances of 0.315 nm and 0.281 nm can be clearly seen, corresponding to the $[\bar{1}2\bar{1}]$ and $[1\bar{2}\bar{7}]$ planes of Ti_8O_{15}. The results are further confirmed by the corresponding FFT pattern (see inset in Figure 2F).

The details of the chemical state and electronic state of the as-prepared Ti_8O_{15} NWs were probed by X-ray photoelectron spectroscopy (XPS). **Figure 2**G shows the comparison of the Ti-2p XPS spectra of Ti_8O_{15} NWs and TiO_2. The curve fitting was done to the peaks of the Ti-2p XPS spectra of Ti_8O_{15} NWs and TiO_2. Two peaks with binding energies at 464.5 and 458.6 eV correspond to the characteristic Ti-$2p_{1/2}$ and Ti-$2p_{3/2}$ peaks of Ti^{4+} for both samples.[25] For the Ti_8O_{15} NWs, there are two extra peaks with binding energies at 463.7 and 458.0 eV, which are consistent with the characteristic Ti-$2p_{1/2}$ and Ti-$2p_{3/2}$ peaks of Ti^{3+}.[25] The comparison of O-1s XPS spectra of Ti_8O_{15} NWs and TiO_2 is shown in **Figure 2**H. The peak at 530.1 eV is related to the Ti-O-Ti.[26] A strong additional peak at 532.0 eV in Ti_8O_{15} NWs is assigned to Ti−OH bond, which is attributed to the hydrogen atmosphere.[27] While no obvious Ti−OH bond in the TiO_2 was found.

High electrical conductivity of the Ti_8O_{15} has been predicted because its narrow forbidden band width results in the transitions of electron from the valence band to the conducting band based on the density functional theory (see Figure S2 and S3 for details). The practical electrical resistance and I–V curve of a single Ti_8O_{15} nanowire are shown in Figure S4. According to its length and diameter, it can be tentatively calculated that the electrical conductivity of the nanowire is 20.6 S/cm at room temperature. Compared with the traditional transition metal oxide nanowires, the conductivity of the Magnéli phase Ti_8O_{15} nanowires is very high.[25-27]

It is worth notice that we did not use any catalyst during the synthesis process of the Ti_8O_{15} NWs, indicating that the growth of Ti_8O_{15} NWs is not dominated by the vapor-liquid-solid (VLS) mechanism. Based on above observation and discussion, a modified vapor-solid (VS) mechanism is proposed to explain the growth mechanism of the Ti_8O_{15} NWs.[28,29] Figure S1 shows the schematic diagram of the experimental spparatus for growth of Ti_8O_{15} NWs. A quartz boat loaded pure TiO_2 powders (99.0%, 5-10 nm, 2 g) was placed at the center of the tube (high temperature region (HT)) and the Ti substrate located 6 cm away from the boat (low temperature region (LT)). Scheme 1 presents the growth process of the Magnéli phase Ti_8O_{15} nanowires. A layer of titanium oxide film (2-5 nm) was formed after the pre-treatment of the Ti foil substrate. When the temperature increases to 1050 °C, the TiO_2 powders in the quartz boat at the center of the tube were reduced to form H_2O (g), the H_2O (g) was transported to the Ti substrate in the LT region, where the H_2O (g), H_2 (g) reacted with the Ti on the Ti substrate to form Ti_8O_{15}. At the beginning, a layer of compact Ti_8O_{15} club-shaped nanoparticles were formed on the Ti foil substrate (Figure S5). The club-shaped Ti_8O_{15} nanoparticles gradually grew into Ti_8O_{15} NWs with the heating time.

Journal Name RSCPublishing

COMMUNICATION

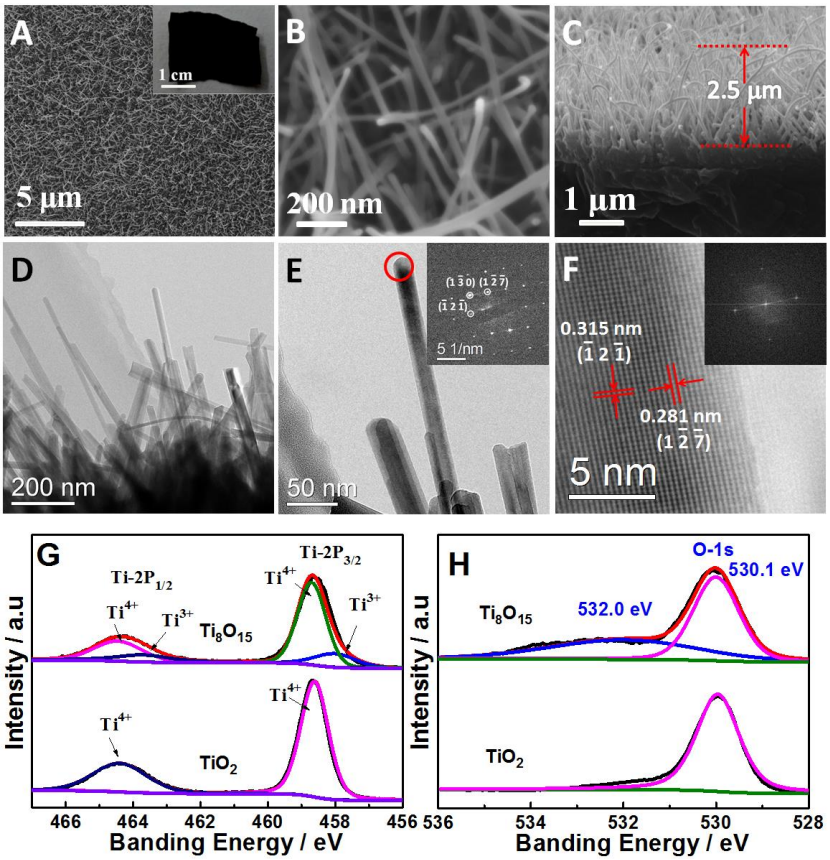

Figure 2. (A,B) SEM images of the Ti_8O_{15} NWs grown on titanium substrate, the inset in (A) is the digital image of the product, (C) SEM image of the cross-section of the Ti_8O_{15} NWs. Given that the Ti_8O_{15} NWs is approximately 2.5 μm, (D,E) TEM images of the Ti_8O_{15} NWs, (F) HRTEM image of Ti_8O_{15} NWs and the corresponding fast Fourier transform (FFT) (inset) and (G,H) Ti-2p and O-1s XPS spectra of Ti_8O_{15} NWs and TiO_2.

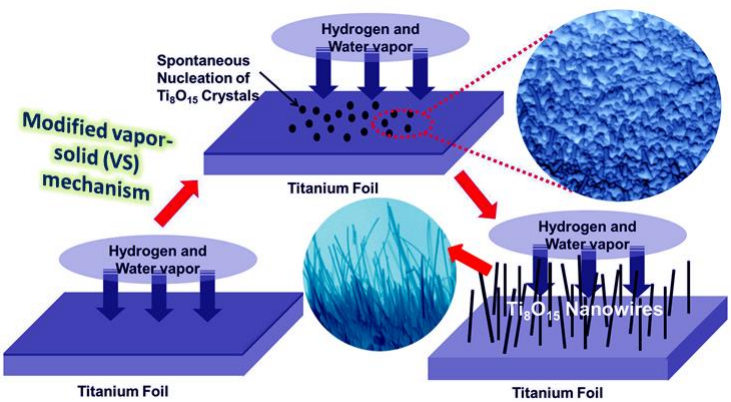

Scheme 1. Schematic illustration of the VS process for Ti_8O_{15} NWs growth.

Journal Name

RSCPublishing

COMMUNICATION

The Magnéli phase Ti_8O_{15} nanowires were used as a carbon-free support to prepare Pt-based catalyst (Pt/Ti_8O_{15} NWs). The Pt/Ti_8O_{15} NWs electrocatalyst was prepared by a electrochemical deposition method (the details are shown in Supporting Information). **Figure 3**A shows the TEM image of the Pt/Ti_8O_{15} NWs. The Pt nanoparticles are uniformly anchored on the Ti_8O_{15} NWs surface. **Figure 3**B and 3C display the HRTEM image of Pt/Ti_8O_{15} NWs, showing the lattice fringes of Ti_8O_{15} NWs and Pt nanoparticles, respectively. **Figure 3**D shows the high-angle annular dark-field scanning transmission electron microscopy (HAADF-STEM) image of Pt/Ti_8O_{15} NWs. The elemental mapping analysis of Ti and Pt using STEM-energy-dispersive spectroscopy (STEM-EDS) obtained from the red box in the **Figure 3**D revealed the uniform distribution of Pt on the Ti_8O_{15} NWs surfaces (**Figure 3**E and 3F) which is consistent with the results of the HRTEM and HAADF-STEM analysis.

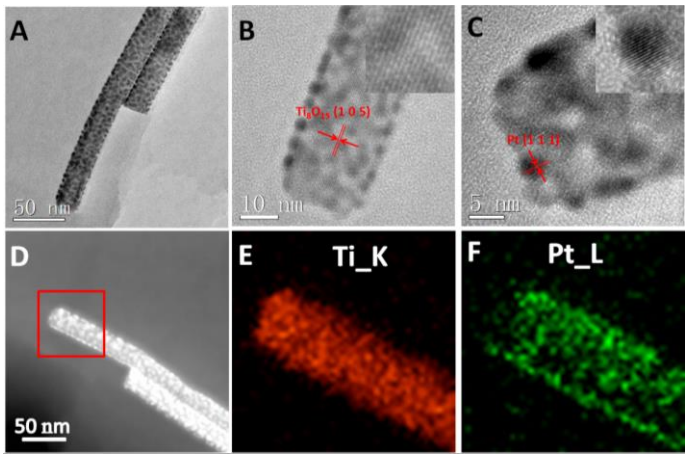

Figure 3. (A) TEM image of Pt/Ti_8O_{15} NWs, (B,C) HRTEM images of Pt/Ti_8O_{15} NWs, (D) HAADF-STEM image of Pt/Ti_8O_{15} NWs, (E,F) HAADF-STEM-EDS elemental mapping images of Pt/Ti_8O_{15} NWs.

The cyclic voltammograms (CVs) in N_2-saturated 0.5 mol L^{-1} H_2SO_4 of the activated catalysts are dispalyed in Figure S6, showing typical Pt characteristics and no other additional current peak was seen, indicating that Ti_8O_{15} NWs has sufficient electrical conductivity and electrochemical inertness as the catalyst support for a MOR electrode. The electrochemical active surface area (ECSA) of Pt/C and Pt/Ti_8O_{15} NWs were almost same, which is likely due to the particle size and Pt loadings of Pt/C and Pt/Ti_8O_{15} NWs are the same. The methanol oxidation reaction (MOR) performances of the Pt/C and Pt/Ti_8O_{15} NWs are shown in **Figure 4**. The peak current densities of the three electrodes are 28.2 mA cm^{-2} for Pt/Ti_8O_{15} NWs, 20.5 mA cm^{-2} for Pt/C and 17.2 mA cm^{-2} for Pt/TiO_2, suggesting that the Pt/Ti_8O_{15} NWs electrocatalyst displays best performance for MOR. Furthermore, the onset potential of the Pt/TiO_2 is positively shifted 60 mV compared to Pt/C and Pt/Ti_8O_{15} NWs. The anti-poisoning abilities of the electrocatalysts were evaluated by a steady-state measurement. The respective chronopotentiometric curves for methanol oxidation on Pt/C and Pt/Ti_8O_{15} NWs electrodes at current density of 5 mA cm^{-2} are shown in **Figure 4**B. On the Pt/C electrode, the potential oscillation appeared during the constant current polarization, indicating the deterioration and poisoning due to the formation of CO-like intermediates on the surface of platinum which need higher potentials to oxidize the CO-like intermediates and release a clean surface.[30,31] While, on the Pt/Ti_8O_{15} NWs electrode, a smooth curve was observed without oscillation, indicating a poisoning-free process for methanol oxidation. The results proved that the Magnéli phase Ti_8O_{15} nanowires supported Pt catalyst is much stable than that of commercial Pt/C catalysts. The durability of the catalyst was further tested by long-time cycling the electrode.

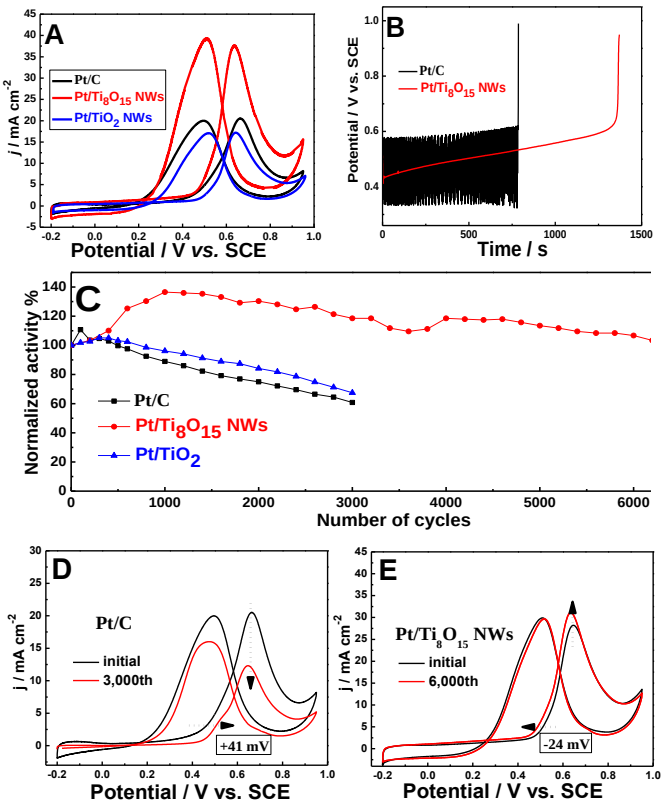

Figure 4. (A) Cyclic voltammograms of Pt/TiO_2, Pt/C and Pt/Ti_8O_{15} NWs electrocatalyst in 0.5 mol L^{-1} H_2SO_4 +1.0mol L^{-1} CH_3OH at 30℃, (B) the chronopotential curves of of Pt/C and Pt/Ti_8O_{15} NWs electrocatalysts, (C) comparison of the peak current

density changing with cycle time for the Pt/TiO_2, Pt/C and Pt/Ti_8O_{15} NWs and (D, E) MOR performance on Pt/C and Pt/Ti_8O_{15} NWs electrode before and after cycling testing.

The potential cycling was performed in the potential range between -0.2-0.95 V (*vs.* SCE). **Figure 4**C shows the comparison of the degradation of the Pt/TiO_2, Pt/C and Pt/Ti_8O_{15} NWs catalysts in normalized activity. In the case of Pt/TiO_2 and Pt/C, the curves were kept continuously decreasing. After 3,000 cycles, the normalized activity is only 60 % for Pt/C and 60 % for Pt/TiO_2. The degradation reached almost half of the original activity. On the other hand, the Pt/Ti_8O_{15} NWs showed a continuous increase in the normalized activity at first 1,000 cycles, then, the normalized activity decreases slowly. However, after 6,000 cycles, the normalized activity is still higher than 100%. **Figure 4**C is only shown the comparison of the normalized activity stability. However, it was further found that the peak current density decreased after 3,000 cycles on Pt/C electrode and the onset potential moved towards negative side by 41 mV (**Figure 4**D). While, on the Magnéli phase Ti_8O_{15} nanowires supported Pt catalyst, the onset potential moved towards negative about 24 mV and the peak current density is higher than the original value after 6,000 cycles (**Figure 4**E). The MOR activity loss of the Pt particles during the cycling performance is attributed to the Pt particle dissolution and subsequent agglomeration to yield larger particles result from Ostwald ripening.[33,34] Oxygen vacancies in Ti_8O_{15} NWs generate a population of surface electrons available for conduction, which enhance the MOR activity and the durability.[35] Oxygen-deficient TiO_2 nanostructure (Ti_8O_{15} NWs) has hypo-d-electron character and could have the ability to interact with Pt that has hyper-d-electron character, leading to electronic interaction between the support (Ti_8O_{15} NWs) and the Pt nanoparticles. This character do not exist in stoichiometric TiO_2, which result in higher durability of Ti_8O_{15} NWs than TiO_2.[36,37] This is in agreement with the results in previous literatures.[6,38,39] The morphology and structure of the Pt/Ti_8O_{15} NWs catalyst after 6,000 cycles was observed by TEM (Figure S7). The one-dimension nanowires structure of the Ti_8O_{15} was remained and the Pt particles show no obvious particle coalescence and aggregation. But, it must be true that the microstructure of the sample has been dredged after cycling which results in the increase in the activity. In the further work, we will do the microscopic and spectroscopic measurements before and after cycling to find the origin of change.

Conclusions

In summary, we have demonstrated that the single-crystalline conductive Magnéli phase Ti_8O_{15} nanowires can be fabricated by a facile one-step evaporation-deposition synthesis method. These Ti_8O_{15} NWs are nanostructured (~30 nm) and excellent in electrical conductivity (20.6 S/cm). The electrochemical properties of the Ti_8O_{15} NWs were also studied by loading Pt nanoparticls as catalyst for methanol oxidation reaction. It is evidenced that the Pt/Ti_8O_{15} NWs catalyst has an enhanced activity and extraordinary high durability for direct methanol oxidation.

Acknowledgement

This work was supported by the Major International (Regional) Joint Research Project of NNSFC (51210002) and the link project of the National Natural Science Foundation of China, Guangdong Province (U1034003) and Guangzhou Automobile Group Project.

Notes and references

[1] *State Key Laboratory of Optoelectronic Materials and Technologies, School of Physics and Engineering, Sun Yat-sen University, Guangzhou, 510275, PR China.*

[2] *Automotive Engineering Institute, Guangzhou Automobile Group Co., Ltd, Guangzhou, 510640, PR China.*

[†] *These authors contributed equally to this work.*

** e-mail: stsspk@mail.sysu.edu.cn; huangxd@gaei.cn.*

Electronic Supplementary Information (ESI) available: Additional data for the characterization and experiment details. See DOI: 10.1039/c000000x/

1 J. R. Smith, F. C. Walsh, R. L. Clarke, *J. Appl. Electrochem.* 1998, **28**, 1021-1033.
2 K. Kolbrecka, J. Przyluski, *Electrochim. Acta* 1994, **39**, 1591-1595.
3 A. D. Inglis, Y. L. Page, P. Strobel, C. M. Hurd, *J. Phys. C Solid State Phys.* 1983, **16**, 317.
4 X. Chen, L. Liu, P. Y. Yu, S. S. Mao, *Science* 2011, **331**, 746-750.
5 W.-Q. Han, X.-L. Wang, *Appl. Phys. Lett.* 2010, **97**, 243104.
6 T. Ioroi, H. Senoh, S.-i. Yamazaki, Z. Siroma, N. Fujiwara, K. Yasuda, *J. Electrochem. Soc.* 2008, **155**, B321-B326.
7 A. Kitada, G. Hasegawa, Y. Kobayashi, K. Miyazaki, T. Abe, K. Kanamori, K. Nakanishi, H. Kageyama, *RSC Advances* 2013, **3**, 7205.
8 S. Tominaka, Y. Tsujimoto, Y. Matsushita, K. Yamaura, *Angew. Chem. Int. Ed.* 2011, **50**, 7418-7421.
9 F. C. Walsh, R. G. A. Wills, *Electrochim. Acta* 2010, **55**, 6342-6351.
10 C. Acha, M. Monteverde, M. Nñúez-Regueiro, A. Kuhn, M. A. Alario Franco, *Eur. Phys. J. B* 2003, **34**, 421-428.
11 A. Kitada, G. Hasegawa, Y. Kobayashi, K. Kanamori, K. Nakanishi, H. Kageyama, *J. Am. Chem. Soc.* 2012, **134**, 10894-10898.
12 Y. Lu, Y. Matsuda, K. Sagara, L. Hao, T. Otomitsu, H. Yoshida, *Adv.Mater. Res.* 2011, **415-417**, 1291-1296.
13 S. Perera, N. Zelenski, E. G. Gillan, *Chem. Mater.* 2006, **18**, 2381-2388.
14 W.-Q. Han, Y. Zhang, *Appl. Phys. Lett.* 2008, **92**, 203117.
15 Y.-J. Wang, D. P. Wilkinson, J. Zhang, *Chem. Rev.* 2011, **111**, 7625-7651.
16 W. Setthapun, S. K. Bej, L. T. Thompson, *Top. Catal.* 2008, **49**, 73-80.

17 M. K. Jeon, H. Daimon, K. R. Lee, A. Nakahara, S. I. Woo, *Electrochem. Commun.* 2007, **9**, 2692-2695.
18 Z. Kónya, V. F. Puntes, I. Kiricsi, J. Zhu, J. W. Ager, M. K. Ko, H. Frei, P. Alivisatos, G. A. Somorjai, *Chem. Mater.* 2003, **15**, 1242-1248.
19 S. J. Yoo, T.-Y. Jeon, K.-S. Lee, K.-W. Park, Y.-E. Sung, *Chem. Commun.* 2010, **46**, 794.
20 K. Senevirathne, R. Hui, S. Campbell, S. Ye, J. Zhang, *Electrochim. Acta* 2012, **59**, 538-547.
21 X. Cui, J. Shi, H. Chen, L. Zhang, L. Guo, J. Gao, J. Li, *J. Phys. Chem. B* 2008, **112**, 12024-12031.
22 Y. Liu, W. E. Mustain, *J. Am. Chem. Soc.* 2013, **135**, 530-533.
23 K.-W. Park, K.-S. Seol, *Electrochem. Commun.* 2007, **9**, 2256-2260.
24 M. Gratzel, *Nature* 2001, **414**, 338-344.
25 Z. Song, J. Hrbek, R. Osgood, *Nano Lett.* 2005, **5**, 1327-1332.
26 G. Lu, S. L. Bernasek, J. Schwartz, *Surf. Sci.* 2000, **458**, 80-90.
27 X. Lu, G. Wang, T. Zhai, M. Yu, J. Gan, Y. Tong, Y. Li, *Nano Lett.* 2012, **12**, 1690-1696.
28 Z. W. Pan, Z. R. Dai, Z. L. Wang, *Science* 2001, **291**, 1947-1949.
29 J. Zhou, N. S. Xu, S. Z. Deng, J. Chen, J. C. She, Z. L. Wang, *Adv. Mater.* 2003, **15**, 1835-1840.
30 M. Krausa, W. Vielstich, *J. Electroanal. Chem.* 1995, **399**, 7-12.
31 P. Justin, G. Ranga Rao, *Int. J. Hydrogen Energy* 2011, **36**, 5875-5884.
32 M.-C. Tsai, T.-K. Yeh, C.-H. Tsai, *Int. J. Hydrogen Energy* 2011, **36**, 8261-8266.
33 S.-Y. Huang, P. Ganesan and B. N. Popov, *Appl. Catal., B : Environ.*, 2010, **96**, 224-231.
34 J. N. Tiwari, K. Nath, S. Kumar, R. N. Tiwari, K. C. Kemp, N. H. Le, D. H. Youn, J. S. Lee and K. S. Kim, *Nat. Commun.*, 2013, **4**, 2221.
35 F. Shi, L. R. Baker, A. Hervier, G. A. Somorjai and K. Komvopoulos, *Nano Lett.*, 2013, **13**, 4469-4474.
36 L. M. Vračar, N. V. Krstajić, V. R. Radmilović and M. M. Jakšić, *J. Electroanal. Chem.*, 2006, **587**, 99-107.
37 B. Babić, J. Gulicovski, L. Gajić-Krstajić, N. Elezović, V. R. Radmilović, N. V. Krstajić and L. M. Vračar, *J. Power Sources*, 2009, **193**, 99-106.
38 T. Ioroi, Z. Siroma, N. Fujiwara, S.-i. Yamazaki and K. Yasuda, *Electrochem. Commun.*, 2005, **7**, 183-188.
39 C. Zhai, M. Zhu, D. Bin, H. Wang, Y. Du, C. Wang and P. Yang, *ACS Appl. Mater. Interfaces*, 2014, **6**, 17753-17761.